Arnold family in acoustically forced air bubble formation

A. Tufaile[1,2] and V. S. Mendes[2], J. C. Sartorelli[2] &, E. Colli[3]

[1]*Universidade de São Paulo, Escola de Artes,*

Ciências e Humanidades Av. Arlindo Bettio 1000, CEP 03828-000 São Paulo, Brazil.

[2]*Universidade de São Paulo, Instituto de Física Caixa Postal 66318,*

CEP 05315-970 São Paulo, Brazil. and

[3]*Universidade de São Paulo, Instituto de Matemática e*

Estatística R. do Matão 1010, CEP 05508-090 São Paulo, Brazil.

Abstract

We applied an integrate-and-fire model with sinusoidal baseline and constant threshold to describe air bubble formation periodically forced by a sound wave. The model is a deterministic one-dimensional system that predicts the instant of a bubble detachment as a function of the previous one and it is able to reproduce long time behavior with great qualitative similarity. The changes in the dynamics as the air flow varies can be predicted by a curve in the parameter space of the so called Arnold family of circle maps.

PACS numbers: 05.45.Ac, 05.45.Pq, 47.55.Dz

Keywords: chaos, integrate-fire dynamics, bubbles

INTRODUCTION

Bubbling from a nozzle submerged in a viscous liquid presents many nonlinear features such as period doubling, period adding bifurcations, and chaotic behavior. The air bubble formation depends on geometrical parameters of the pneumatic system [1, 2], such as the hose length connecting the air flow control system to the nozzle, its diameter and chamber volume, and the liquid column height. But it also depends on the fluid properties such as the liquid viscosity and the surface tension at the interface of the two phases.

The main and simplest outcome from this experiment is the temporal series of time intervals between bubbles, that can be measured with the aid of a laser beam. Notwithstanding the complexity of the two-phase flow phenomenon, it is often possible to reproduce this series, at least from the qualitative point of view, by generating the instants of bubble detachment with a deterministic iterated map with few degrees of freedom. This brings the theory of dynamical systems as a tool to understanding some hydrodynamical phenomena.

Regardless the purely abstract interest in the

richness of chaotic patterns, there are technological applications of bubbling systems in many areas, from everyday situations to industry, that brought some researchers to study the transitions of bubbling regimes subject to a control parameter ([3]) *(o que tem exatamente nesta referência?)*. Sarnobat et al ([4]) studied the effects of electrostatic fields in bubble formation and Ruzicka et al ([5]) experimentally found the adverse effect of the liquid viscosity on the stability of the regular regime for aqueous glycerol solutions. Even in a champagne glass these transitions between bubbling regimes can be observed during the degassing process ([11, 12]).

We studied the bubble formation generated in a nozzle submerged in water/glycerol solution inside a cylindrical tube, submitted to a sound wave tuned in the air column above the fluid (previous results with this setting were reported in [6–9]). The data are mainly collected in the following way: the air flow rate, which is the control parameter, is slowly increased and time intervals between bubbles are plotted against the flow. This is a quick method for generating the bifurcation diagram of the dynamics under the influence of the control parameter. All other parameters, like the amplitude of the sound wave, are kept fixed along each individual experiment. Other bifurcation diagrams are obtained with different settings of the fixed parameters.

We compared the experimental bifurcation diagrams with those obtained with a deterministic model, whose origin is in an integrate-and-fire argument. We assumed that the bubble volume (or any other quantity, like the radius or the pressure) grows linearly with time, with a coefficient α that depends on the air flow rate Q (this dependence will be discussed later). We supposed that the starting volume of the growth process at instant t_n is determined by the value of the baseline $b(t)$, see Fig. 1, that is a sinusoidal function $b(t) = -A\sin(2\pi f_s t)$, where the minus sign is for later convenience, f_s is the frequency of the sound wave, and $A > 0$ is a factor related to its amplitude. Defining $\tau = f_s t$ means that the time scale is normalized so that one unit corresponds to the period of the sound wave. Now the baseline is given by $b(\tau) = -A\sin(2\pi\tau)$. The detachment of the bubble occurs at instant τ_{n+1}, when the volume reaches a certain critical value V_c. The constant function $V(\tau) = V_c$ is the threshold in this model. Therefore, τ_{n+1} and τ_n are related by

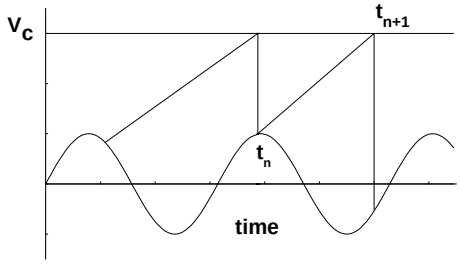

FIG. 1: The integrate and fire dynamics model with the sinusoidal bubbles initial conditions drive by the sound wave.

$b(\tau_n) + \alpha(\tau_{n+1} - \tau_n) = V_c$, which gives

$$\tau_{n+1} = G(\tau_n) = \tau_n + f_s\alpha^{-1}(V_c + A)\sin(2\pi\tau_n).$$

The map G is a member of the two-parameter family

$$G_{\Omega,\epsilon}(\tau) = \tau + \Omega + \epsilon\sin(2\pi\tau),$$

known as the Arnold family (see [13] or [de Melo & van Strien]).

Iteration of the map gives the instants τ_n of bubble detachments, but in general one is interested in the sequence of phases $\tau_n \bmod 1$. A periodic regime of period p, for example, occurs when $\tau_{n+p} = \tau_n \bmod 1$ in the long term behavior. Here we are more interested in the sequence of time intervals $R_n = \tau_{n+1} - \tau_n$. It is easy to see that period p in the above sense implies that R_n is also periodic with the same period, although the converse statement is not necessarily true. It also implies that $\sum_{i=0}^{p-1} R_{n+i}$ is an integer value.

An idea of the variety of behavior of the Arnold family can be obtained by a diagram in the (Ω, ϵ) parameter space with colors informing the regions for which each one of the behaviors occurs, including non-periodic and/or chaotic ones. Due to their shape, the parameter regions corresponding to periodic behavior for low values of ϵ received the name of Arnold tongues.

In Ref. [7], maps like those of the Arnold family have been also used to describe the dynamical phenomena appearing in bubble formation under sound influence, as an *ad hoc* approach based on similarity of qualitative behavior. Here, in turn, we were not only able to motivate that approach with physical heuristics, but we gave a much more precise description involving some experimental parameters, namely the air flow and the amplitude of the sound wave.

Integrate and fire dynamics with sinusoidal oscillation in the threshold, instead of the initial conditions baseline, has also been used to model certain aspects of neurons ([14]), cardiac rhythms ([?]), sawtooth oscillations in some electronic circuits [?], and impact oscillators ([15]). For higher values of α in our model, changing the sinusoidal oscillation from the baseline to the threshold does not imply a qualitative change of the behavior. But for low values of α there may be tangencies between the growing function and the threshold that lead to discontinuities of the map G (a discussion of integrate-and-fire models, with general baselines and thresholds, is given in [???Tufa me mostrou artigo]) that are not observed in the experiment. Moreover, a map G coming from an integrate-and-fire model with constant baseline cannot have turning points, like those of the Arnold family for $\epsilon > \frac{1}{2\pi}$. This implies that constant baselines are not able to reproduce the chaotic behavior and period doubling bifurcations that the experiment shows.

Integrate-and-fire models with sinusoidal baselines have been considered also in [13] and [14] *conferir isto*. *(O que tem no ?* [10]*)*;

RESULTS AND DISCUSSION

The air bubble formation experimental apparatus is shown in Fig. 2. The bubbles are generated by injecting air through a metallic nozzle submerged in a viscous fluid column placed in a cylindrical tube. The air flow is controlled by a proportional solenoid valve which is driven by a PID controller. We detected the voltage pulses induced in a resistor when the bubbles cross a laser beam placed a little above the nozzle, and the delay times $T_n = t_{n+1} - t_n$ between successive bubbles were measured with a time circuitry inserted in a PC slot, with a time resolution equal to $1\mu s$. The total experimental noise was estimated as $100\mu s$ (see [Sarto94,Tufa99] for details). By applying a sound wave with a loud-speaker placed at the top of the tube, and tuned to the fundamental frequency ($f_s = 135Hz$) of the air column above the liquid, a small part of the wave is refracted to the liquid. Despite the very small refracted wave amplitude ([20]), it is enough to produce huge changes in the bubble formation dynamics ([7]). We have constructed experimental bifurcation diagrams of $R_n^{\exp} = f_s T_n$ versus Q, where Q is the air flow, for four values of the sound amplitude (2, 4, 6, and 8V measured in the output of the function generator), letting the air flow Q to increase in a linear ramp mode at the rate of $\sim 12ml/min^2$. All the measures were done at room temperature.

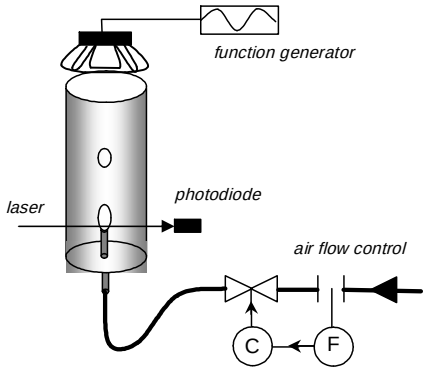

FIG. 2: Diagram of the experimental apparatus.

In a regular regime the mean bubbling time behave as $< T > \sim Q^{-\beta}$ (see [???]; such relation was also observed in water drop formation [18, 19]). In the present work the experimental exponent is $\beta \approx 0.4$ in the range $[40, 100]ml/min$, although for $Q \sim 90ml/min$ the relation starts to deviate from this scale law due to nonlinearities that come from the influence of a bubble detachment in the next one (see Fig. 4 of [1]). On the other hand, in the model this mean time $< T >$ is approximately V_c/α, meaning that we may substitute this term by $V_c Q^{-\beta}$. Also, the factor A/α may be substituted by $AQ^{-\beta}$. At the end, we have the model for the simulations

$$t_{n+1} = G(t_n) = t_n + Q^{-\beta}(V_c + A\sin(2\pi t_n)),$$

and the relation with the Arnold family para-

meters now is given by $\Omega = f_s V_c Q^{-\beta}$ and $\epsilon = f_s A Q^{-\beta}$.

The constants V_c, A, and β, in cgs units, were obtained from the experimental data. In the theoretical setting, for fixed values of these parameters, we see that $R_n = f_s(t_{n+1} - t_n)$ must be in the interval $[f_s(V_c - A)Q^{-\beta}, f_s(V_c + A)Q^{-\beta}]$ which gives the thickness of the diagram. We suppose that for certain values of Q the non-periodic behavior is such that the values R_n distribute themselves all over this interval, allowing us to determine its boundary points. In the simulation we also tried to reproduce the conditions of the experiment, by summing up at each iteration a random noise uniformly distributed in the interval $[-100, 100]\mu s$

For each one of the four bifurcation diagrams we have done an independent qualitative fitting of the three constants, although in principle β and A should remain constant independently of the amplitude of the sound wave. The fitting was based on least square for determining β and V_c, and visual comparison to find A and adjust V_c. The criteria were the diagram thickness, position and width of the plateaus. At the end the values of β and V_c underwent relatively small changes in the four experiments, and as expected A values grew with the amplitude of the sound wave.

In Fig. 3(a) is shown the experimental bifurcation diagram $R^{\exp}$ vs. Q with sound amplitude $2V$ and in Fig. 3(b) the corresponding simulation for R^{sim}. There we can observe the period 1 plateaus at integer values of R_n in both cases. It may be interpreted as a frequency locking between the cycle of bubble formation and the sound wave, when the dripping rates are submultiples of the sound frequency.

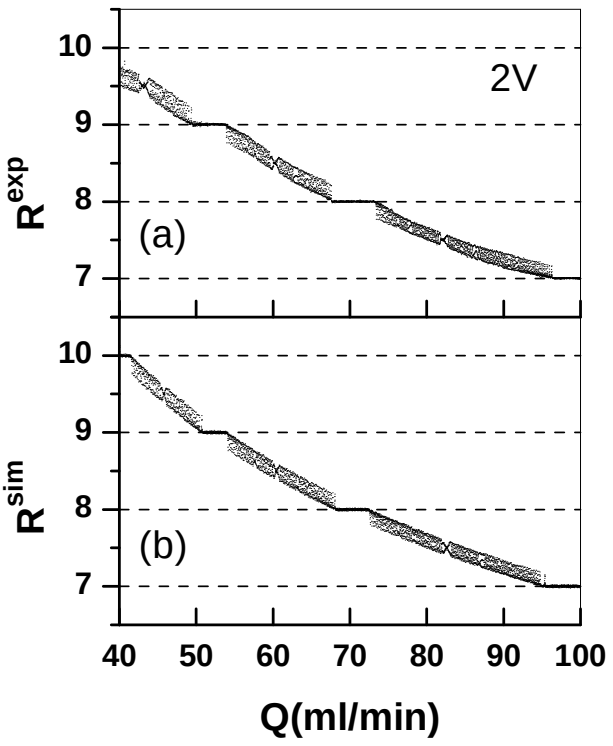

FIG. 3: (a) Experimental bifurcation diagram for $2V$ sound wave amplitude. (b) Simulation with $A = 0.75 \times 10^{-3}$, $V_c = 0.0631$ and $\beta = 0.40$. The experimental frequency lockings are well reproduced for k=integer numbers as well as for k=half integers.

It is worthwhile noting that a period 1 plateau seems to appear in the lower envelope of the experimental diagram and disappear at the upper one, defining the diagram thickness where non periodic R_n are distributed. This is fully con-

firmed by the model since the lower envelope is attained by R_n whenever $\sin(2\pi\tau_n)$ is minimum and the upper ones whenever $\sin(2\pi\tau_n)$ is maximum.

On the other hand, the period 1 appears and disappears associated to tangencies between the graphs of $G(\tau)$ and $\tau + k$, that happen exactly at the critical points of the sine function. As Q increases, the graph of G goes down, and the first tangency is at a minimum of the sine function. An immediate consequence is that the width of a plateau at level k is given by:

$$((V_c + A)/k)^{1/\beta} - ((V_c - A)/k)^{1/\beta},$$

that is, the plateaus are smaller for higher values of k.

In between the plateaus there are also other kinds of behavior related to higher periods. The most visible of them is the period 2 regime, between the plateaus k and $k + 1$, where R alternates between two values whose mean value is $k+1/2$, hence this subharmonic frequency locking can be seen in the bifurcation diagrams at half-integer levels.

In Fig. 4(a) we see the bifurcation diagram R^{exp} $vs.$ Q for sound wave amplitude equal to $4V$, with the corresponding simulation R^{sim} $vs.$ Q in Fig. 4(b). We first note that A significantly increased, contrary to V_c and β, that assumed values near the fitting of the previous diagram. In comparison with a lower value of amplitude, the thickness of the diagram and the width of the plateaus increased, as predicted by the model. Also the width of the period-two windows at half-integers levels increased; and period 3 appeared (around $80ml/min$) between $k = 7$ and $k = 8$ with R alternating between 3 values whose mean values $\sum_{i=0}^{2} R_{n+i}/3$ are $22/3$ and $23/3$.

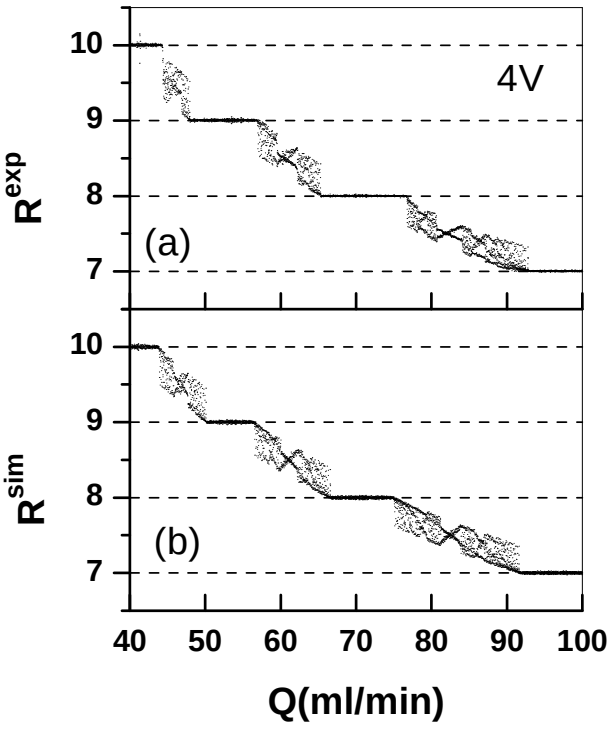

FIG. 4: (a) Experimental bifurcation diagram for $4V$ sound wave amplitude. (b) Simulation with $A = 1.42 \times 10^{-3}$, $V_c = 0.0634$ and $\beta = 0.415$. In addition to the experimental frequency lockings well reproduced for k=integer and for k=half integers we can observe period 3 for k=22/3 and k=23/3.

Increasing the amplitude to 6V, as shown in Fig. 5, the plateaus of period 1 $k = 10$ and 9 are not flat anymore, presenting bifurcations

from period 1 to period 2 and after from period 2 back to period 1.

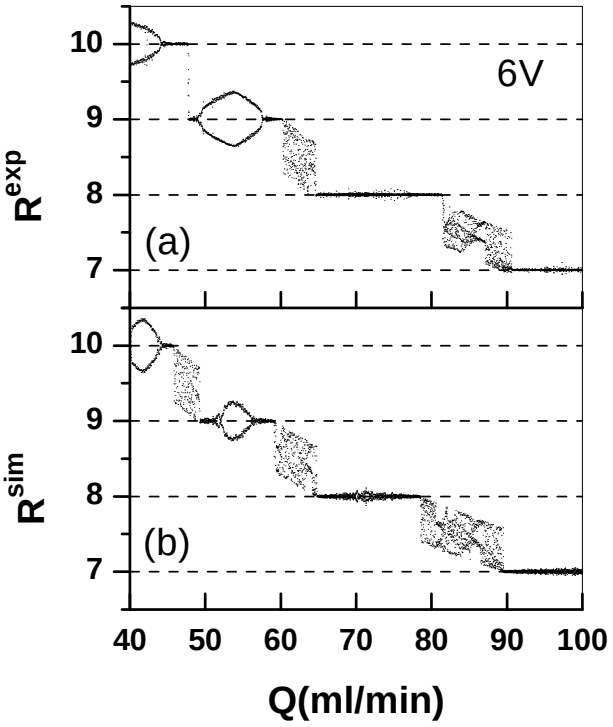

FIG. 5: (a) Experimental bifurcation diagram for $6V$ sound wave amplitude. (b) Simulation with $A = 2.48 \times 10^{-3}$, $V_c = 0.0637$ and $\beta = 0.414$. In this case we can see period 2 related to the addition period bifurcation of the period 1 also reproduced by the simulation.

Increasing even more the sound wave amplitude to 8V, for $k = 10$ and 9 the plateaus also show chaotic behavior, and the complexity of the plateaus propagates through the lower ones, as shown in Fig. 6.

This may be better understood if the four diagrams are seen as cuts of the parameter space (Ω, ϵ) of the Arnold family. With β, V_c, and A kept fixed along each bifurcation diagram, the

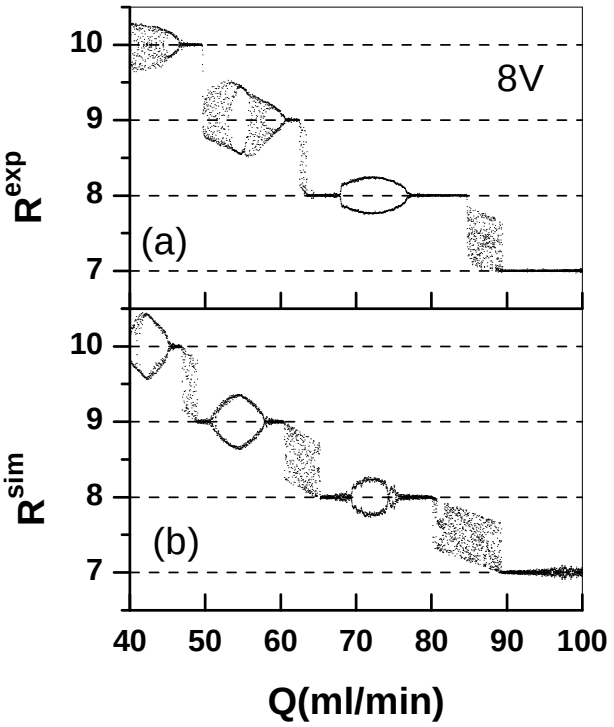

FIG. 6: (a) Experimental bifurcation diagram for $8V$ sound wave amplitude. (b) Simulation with $A = 2.8 \times 10^{-3}$, $V_c = 0.064$ and $\beta = 0.416$. We can see chaotic behavior related to the doubling period in each branch of period 2.

variation of Q may be regarded as the parametrized curve $(\Omega, \epsilon) = (f_s V_c Q^{-\beta}, f_s A Q^{-\beta})$. In this case, the trajectories are segments of straight lines through the origin, with slope equal to A/V_c, with non-uniform velocity. Each one of the four trajectories is shown in Fig. 7 over a diagram showing three parameter regions marked as: wave (blue)=period 1, dotted (red)=period 2, black=period 3, and white regions=the higher periods or non-periodic behavior. The trajectories cross the Arnold tongues,

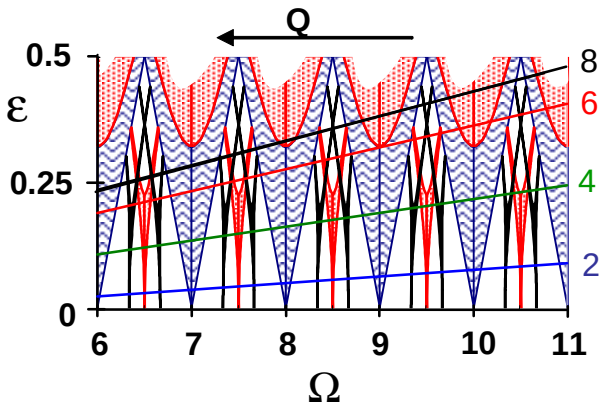

FIG. 7: (Color online) Arnold parameter space. The regions marked as: waves(blue) corresponds to a period 1; dotted (red) period 2, black period 3, and white regions higher periodic and non-periodic behaviors. The trajectories of the four bifurcation diagrams are also shown.

starting from higher to lower values of Ω and ϵ. As the dynamical behavior of the Arnold family is more complex for higher values of ϵ, it becomes clear the relation between the qualitative behavior at the plateaus and the values of the amplitude and air flow rate.

CONCLUSIONS

We studied the effects of the sound wave in the bubble formation from a nozzle submerged in a viscous fluid. Using time measurements as a function of the air flow rate, for different values of the sound amplitude, we captured one of the main aspects of this system, which is that the beginning of the cycle of bubble formation is controlled by the sound wave. From this assumption, we proposed a model based on integrate-and-fire dynamics in which the baseline is a sinusoidal function and the threshold is a horizontal line.

Since this model is an element of the Arnold family, it follows that the complex sequence of transitions observed in our experiment, for example harmonic and subharmonic resonances, flat plateaus or even plateaus with period doubling and chaotic behavior, can be explained by curves in the parameter space of the Arnold family.

Acknowledgements: This work was partially supported by Brazilian agencies FAPESP and CNPq.

[1] V. S. M. Piassi, A. Tufaile, J. C. Sartorelli, Chaos **14**, 477 (2004).

[2] E. Colli, V. S. M. Piassi, A. Tufaile, J. C. Sartorelli, Phys. Rev. E **70**, 066215 (2004).

[3] A. A. Kulkarni, J. B. Joshi, Ind. Eng. Chem. Res. **44**, 5873 (2005).

[4] S. U. Sarnobat, S. Rajput, D. D. Bruns, D. W. DePaoli, C. S. Daw, K. Nguyen, Chem.Eng. Sci. **59**, 247 (2004).

[5] M. C. Ruzicka, J. Drahos, P. C. Mena, J. A. Teixeira, Chem. Eng. J. **96**, 15 (2003).

[6] A. Tufaile, J. C. Sartorelli, Phys. Lett. A **275**, 211 (2000).

[7] A. Tufaile, J. C. Sartorelli, Phys. Lett. A **287**, 74 (2001).

[8] A. Tufaile, M. B. Reyes, J. C. Sartorelli, Physica A **308**, 15 (2002).

[9] R. Mosdorf, M. Shoji, Chem Eng. Sci. **58**, 3837 (2003).

[10] R. Perez, L. Glass, Phys. Lett. A **90**, 441 (1982).

[11] G. Liger-Belair, Ann. Phys. (Paris) **27**, 1 (2002).

[12] G. Liger-Belair, A. Tufaile, B. Robillard, P. Jeandet, J. C. Sartorelli, Phys. Rev. E **72**, 037204 (2005).

[13] L. Glass, Nature **410**, 277 (2001).

[14] S. Coombes, Phys. Lett. A **255**, 49 (1999).

[15] A. Pikovsky, M. Rosenblum, J. Kurths, Synchronization, A Universal Concept In Nonlinear Sciences, Cambridge, (2003).

[16] A. Tufaile, J. C Sartorelli, Physica A **275**, 336 (2000).

[17] A. Tufaile, J. C. Sartorelli, Phys. Rev. E **66**, 056204 (2002).

[18] A. Tufaile, R. D. Pinto, W. M. Gonçalves, J. C. Sartorelli, Phys. Lett. A **255**, 58 (1999).

[19] K. Kiyono, N. Fuchikami, J. Phys. Soc. Jpn. **71**, 49 (2002).

[20] Supposing that the sound properties in the liquid is not too much different from the water, the amplitude of the refracted wave is $A_2 = \frac{2r_1}{r_1+r_2}A_1$, where $r_1 = 42.6 dyne \cdot s/cm^3$ and $r_2 = 14800 dyne \cdot s/cm^3$ are the specific acoustic impedances of the air and of the water, respectively.